


Article

Colour Transformation and Textural Change in Biotite: Some Remarks for the Interpretation of Firing Technology in Greyware Pottery Thin-Sections

Esther Travé Allepuz 

Department of History and Archaeology, Universitat de Barcelona, 08001 Barcelona, Spain; esther.trave@ub.edu; Tel.: +34-93-403-79-45

Abstract: Firing is a crucial step in the production of pottery, as it irreversibly transforms the clay into ceramic. Clay sintering and subsequent vitrification occur during firing, together with other transformations undergone by specific minerals and rock inclusions according to their optical and physical properties, including their colour. Some of these are visible in thin-sections and might be interpreted as technological markers or contribute to the estimation of firing temperatures, although most of them are poorly documented. In this paper, we approach the transformations in colour, texture and optical properties that occurred in biotite inclusions from medieval greyware pottery. Our study considers a batch of 40 pottery samples from medieval Catalonia analysed by XRD. According to the estimated firing temperature ranges and atmospheres, we examined the behaviour of biotite at different temperature ranges from 700 °C to 1000 °C by means of optical microscopy, considering its size, shape and abundance, and compared these features to a wider assemblage of thin-sections from medieval earthenware. The results obtained are interesting, as they offer a valuable reference for petrographic studies on pottery. We discuss the potential of ceramic petrography as a way to perform more precise and refined sample selection for further analysis on archaeothermometry.



Citation: Travé Allepuz, E. Colour Transformation and Textural Change in Biotite: Some Remarks for the Interpretation of Firing Technology in Greyware Pottery Thin-Sections. *Minerals* **2021**, *11*, 428. <https://doi.org/10.3390/min11040428>

Received: 22 March 2021

Accepted: 16 April 2021

Published: 18 April 2021

Publisher's Note: MDPI stays neutral with regard to jurisdictional claims in published maps and institutional affiliations.



Copyright: © 2021 by the author. Licensee MDPI, Basel, Switzerland. This article is an open access article distributed under the terms and conditions of the Creative Commons Attribution (CC BY) license (<https://creativecommons.org/licenses/by/4.0/>).

Keywords: XRD; ceramic petrography; biotite; earthenware; firing; birefringence

1. Introduction

Greyware pottery was a ceramic product for daily use and cooking purposes widespread in medieval Catalonia, and almost exclusive in many sites from the 8th to the 13th centuries. In the last decade, the study of these plain undecorated vessels, with their simple and homogeneous shape of boiling pots or 'ollae', revealed the main circuits of production and distribution in Catalonia and their implications in social and economic terms [1,2]. More recently, we studied specific issues of technological processes related to firing and the quality control of the final products [3]. Paradoxically, surface colour is an important feature of these grey vessels. Dull grey to dark brown or black surfaces were expected to have a touch of shiny and glassy appearance that made them more appreciated, particularly in recent periods when their function and shape became more complex and diverse, and wider typologies appeared, as shown in Figure 1. In this case, colour and texture had much to do with firing and the creation of an oxygen-free atmosphere.

The firing process of greyware pottery is traditionally performed in an updraft double-chambered kiln, even though simpler bonfire-like structures are known [4]. Medieval permanent or semi-permanent structures known in Catalonia shared common features in most cases according to the archaeological record. They were kilns with a fire chamber and an access hole usually cut into the bedrock leaving a pierced platform on which the pottery was placed. A firing chamber was usually built above the combustion chamber as a cylindrical brick or adobe wall with a domed roof. The regular size of these kilns oscillated between 1–3 m in diameter during the medieval period, which was the usual standard size in many areas throughout Western Europe [5,6] and increased their size more

recently. Several holes on the roof were used to control the firing process inside the kiln and to regulate the firing atmosphere.



Figure 1. Selection of vessels representative of later periods of greyware pottery in Catalonia. These are pitchers, jars or jugs together with a wine measure, a heating pot and a brazier. All of them were part of the permanent collection at the former Pottery Museum of Quart.

Literature on experimental archaeology [7–9] and, particularly, ethnographic references from traditional greyware potters [10,11] and the use of kilns [12] (pp. 64–74) provide beautiful insight into the firing technology. Nowadays, after loading the pottery into the firing chamber and closing it, the fire starts at a low temperature with small bundles of bush firewood, usually heather, elm leaf blackberry or Mediterranean gorse. A few hours later, usually half a day, potters start loading the fire chamber with firewood to make the temperature rise until c. 960 °C [13] (p. 74). Maximum temperature was a bit lower in the medieval period (850–900 °C). Firewood supply must be sustained at this point in order to ensure that maximum temperature is going to be stable for some hours, until the cargo is completely fired. Potters keep visual control of the vessels to assess the end of the firing stage. Traditional potters working today in Catalonia identify this moment by the vessels' incandescent 'egg-yolk' colour [14] (p. 54).

Then, the reduction process starts. A final load of firewood is placed in the fire chamber and both chambers are completely sealed with bricks and a layer of sand. The complete enclosure of the kiln is assessed by approaching a candle to the possible edges and cracks in the kiln structure through which oxygen might circulate. If any, the potter seals them one by one with some handfuls of clay extended through the kiln surface. The structure is left to cool down during ten or fifteen days. After the cooling period, the fire chamber is opened first and wood-coal removed. Finally, potters open the combustion chamber as well and remove the greyware vessels. According to the kilns excavated in archaeological sites, this process would have been very similar in the medieval period.

Archaeological science has adopted several methods to approach firing technology. Re-firing tests on pottery sherds or experimental samples, and subsequent SEM observation of vitrification structures allow researchers to interpret changes in the texture of clay matrices. Mineralogical characterization of samples using XRD is a useful and commonly used method to approach the degree and temperature of firing. This practice of 'archaeothermometry' [15] (pp. 426–435) relies on the lack or presence of certain mineral phases that form or are lost at specific temperatures [16] and makes use of 'bar diagrams' documenting the firing sequence of a typical pot [17–21]. It is also possible to estimate the firing temperature in s of pottery through the observation of thermally induced changes in the clay matrix [22,23] and specific mineral inclusions [23] (p. 190). In fact, some minerals undergo changes in body colour due to the oxidation of iron at specific ranges of temperature. This happens to serpentinite or glauconite at low temperatures below 600 °C and

to hornblende at a higher temperature (c. 750 °C). Other minerals such as feldspars lose their stability and start melting at temperatures > 1100 °C [23] (p. 191). Perhaps calcite is the most affected mineral in the common range of temperatures for most earthenwares. It transforms from CaCO₃ to CaO at temperatures of c. 650–750 °C and is decomposed at 800–850 °C completely [24]. Recarbonation of CaO after firing expands its volume and can lead the pot to collapse. The effects in the use of calcareous clay or non-calcareous clay with carbonate inclusions and their effect on pottery production has been in the spotlight of archaeological literature [25], and it has been a crucial topic in the technological approach to greyware pottery as well [26].

The alteration of micas is expected to happen at temperatures between 900–1000 °C, but the precise range of temperature at which these changes occur and their nature—colour transformation, loss of birefringence and deformation—are still poorly known [23] (p. 191). Our research on medieval greyware may provide useful insight in order to deal with this topic, particularly with the transformation of biotite mica. Certainly, biotite is a common constituent of silicate bedrock and its weathering is the dominant natural source of potassium in terrestrial ecosystems. This has been a topic of special interest to soil scientists for a long time, and much of the research on mica weathering is found in soil science literature [27–31] rather than in geochemical literature [32,33]. Despite this, the mechanisms of biotite breakdown under pressure and heat conditions—which are closer to those in pottery fabrication than mere weathering reactions—have been widely explored within the domain of metamorphic petrology [34–37]. Shock-induced pressure-dependent transformations concomitant to impact metamorphism can lead to the formation of new minerals such as garnet or vesiculated glass [38], but the most common affectations of this mineral are those related to thermal [39–42] or hydrothermal alteration [43,44].

However, information about the optical implications of such transformation is scarcely known, and it is even more remote in the domain of ceramic petrography. The aim of this paper is to point out the visual transformations occurred in biotite inclusions within pottery in a range of firing temperatures between 700–1000 °C. Biotite inclusions are particularly frequent in medieval greyware pottery from Catalonia. Identifying such processes under the microscope and comparing them to the XRD characterization of the samples, allows us to offer a first-step estimation of temperatures. It can also lead to more precise and refined sampling—as will be discussed throughout this paper—for specific studies on archaeothermometry.

Certainly, microscopic observation of pottery thin-sections is a common and cost-effective technique nowadays extended to most archaeological studies, and it is at the basis of material science [45]. Especially in coarse wares, it contributes to explaining the provenance and technological issues of pottery groups arising from mineralogical or geochemical datasets [46,47]. Counting on accurately described petrographic groups provides valuable information in order to define strategies for sample selection and develop further characterization studies more efficiently. The results obtained allowed us to define visual patterns of biotite transformation or breakdown that we will describe and discuss in this research piece.

2. Materials and Methods

Our study considered a batch of 40 reference pottery samples from medieval Catalonia analysed by XRD. According to the estimated firing temperature ranges and atmospheres, we examined the behaviour of biotite by means of optical microscopy, considering its colour, birefringence, size, shape and abundance, according to the temperature range for each sample. Then, we compared them to a wider assemblage of thin-sections from medieval earthenware. Data related to the origin, macroscopic features, shape and interpreted provenance of these samples have been previously published [1,2]. Appendix A at the end of this paper summarizes archaeological and contextual data for all 40 samples. Figure 2 shows the geological map of Catalonia [48] with sites and samples location.

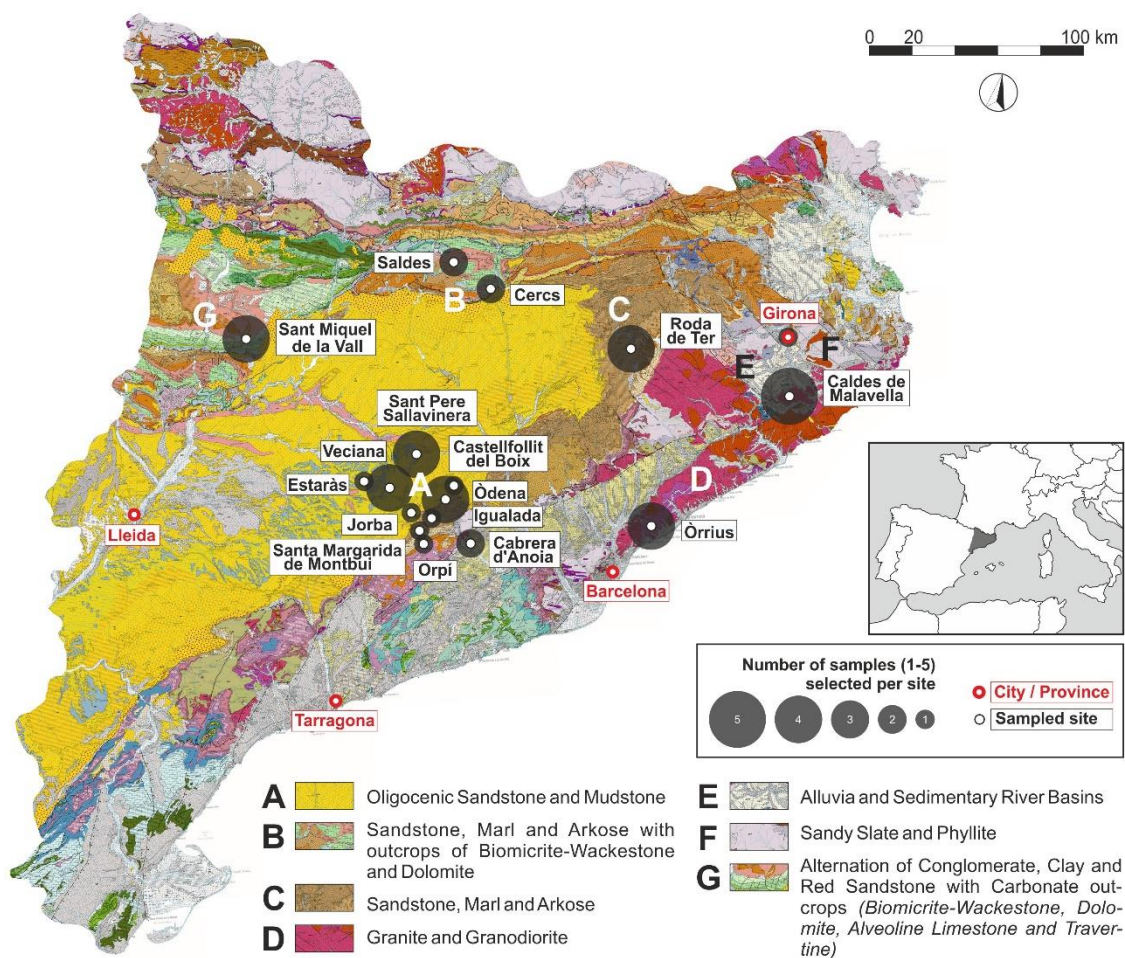


Figure 2. Location map of the samples analysed and the geological environment of the sampled sites. The Geological map of Catalonia is available at the Catalanian Cartographic Institute (ICC: Institut Cartogràfic de Catalunya) website together with its detailed legend [48].

The assemblage is representative of the main medieval greyware pottery productions known in Catalonia, and the petrographic features of all samples are illustrative of the main geological formations in this country as well. Samples have non-calcareous matrices and the presence of calcite is mostly due to the rare occurrence of limestone or marl inclusions in some petrographic fabrics. According to their bulk chemical composition published elsewhere [1,2], they are considered non-calcareous pottery. Standard 30- μm thin-sections of all sherds were prepared within a wider research project including more than 300 pottery sherds that were visually grouped into petrographic fabrics under the polarising light microscope, based upon the nature of their inclusions, clay matrix and voids [23] (pp. 73–79).

We interpreted each fabric in terms of its raw materials and manufacturing technology [1–3]. Samples were subjected to detailed XRD characterization in order to determine their firing temperatures. The analysis was performed at the Wolfson Material Culture and Archaeological Science (MCAS) laboratories of the Institute of Archaeology, University College London, using a Rigaku MiniFlex 600 Benchtop X-ray Diffractometer with power of 0.6 kW (40 kV, 15 mA). Measurement was conducted between 3.0 and 90.0 $^{\circ}2\theta$ using 0.02 $^{\circ}$ step width, at a speed of 10.0 $^{\circ}$ /min in continuous scanning mode. The resulting diffractograms were analysed using Panalytical HighScore-Plus software [49] in order to identify the peaks of reflectance. These were interpreted in terms of the minerals present in the samples using the International Centre for Diffraction Data—Joint Committee of Powder Diffraction Standards, 2006 (ICDD-JCPDS) database. The mineralogical assemblages de-

ected in each sherd were compared with the body of literature that exists on XRD ceramic archaeothermometry [17,18,20,21,50–52]. This allowed us to assess their relative firing conditions and assign an approximate temperature range to each of them [3]. Complementary aspects like the birefringence of the matrix, which is expected to disappear at about 800–850 °C [23] was also considered.

The persistent observation of biotite altered features in the thin-section analysis of medieval greyware pottery led us to search for the systematization of these features according to our interpretation of firing technology. We aimed to determine the difference in colour, birefringence and texture from samples included within one temperature range to another, and to compare whether the changes occurred in biotite and other transformations of clay matrix, inclusions or voids. A detailed record of these issues allowed us to interpret the range of temperatures at which the main transformations take place and the meaning of these changes regarding the technological process of greyware production.

3. Results

Biotite is a trioctahedral mica occurring in a great variety of geological environments and, therefore, quite common in ceramic materials. Biotite inclusions present in greyware pottery sherds from medieval Catalonia are mostly related to granitic or metamorphic bedrocks, which are at the origin of non-plastic inclusions within the paste. Not surprisingly, the amount of biotite inclusions in samples related to fabrics from sedimentary origin is considerably lower. All 40 samples are coarse; they contain a percentage of inclusions counting for 20–40% and were fired under reducing conditions, which was the most-common practice in medieval Catalonia attested by a considerable number of examples from the archaeological record [53,54] and the ethnographic approach [10,11,13]. Accordingly, in this section we will describe the estimation of firing temperatures according to XRD results and the detailed characterization of biotite inclusions of the selected samples in order to discuss the correlation between identified features of biotite and estimated temperature ranges at a further step.

3.1. Estimation of Firing Temperature

The samples analysed via XRD include lower fired (<750 °C) examples in which calcite and mica-type clay minerals such as illite or muscovite are frequent. Although a slightly higher temperature range (<850 °C) might be assumed, the amount and integrity of limestone or marl inclusions together with the moderate to high optical activity of the matrix and easy breakage of hand specimens suggests this low-temperature range. Other lower fired samples reached higher temperatures, but maghemite is absent in all cases. The main mineral assemblage of these samples being illite, quartz, plagioclase and potassium feldspar, firing temperature is estimated at <850 °C due to the constant presence of illite and the absence of maghemite or other high temperature mineral phases. Samples within this group do not include calcite inclusions on a regular basis. Samples including a higher amount of plagioclase and lower illite peaks should be at the limit of c. 900 °C, due to the absence of high temperature minerals. At temperatures of 900–950 °C, quartz, plagioclase, potassium feldspar and maghemite is the common mineral assemblage, and illite peaks—if any—are very low. Illite is completely absent at higher firing temperatures (>950 °C), and sherds classified within this fabric include hercynite. Figure 3 shows a representative diffractogram per fabric and the number of samples included in each group.

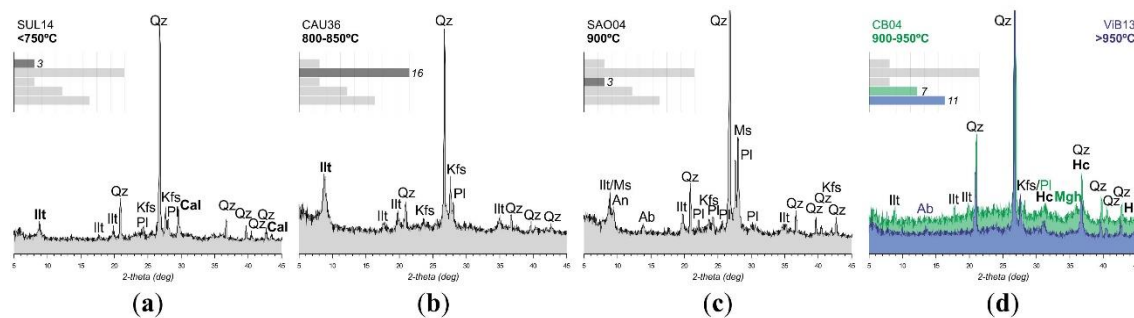


Figure 3. Diffractograms of representative samples for different temperature ranges: <750 °C with stable phases of illite and calcite (a), 800–850 °C still showing illite peaks (b), c. 900 °C with an increasing amount of plagioclase (c) and >900 °C when hercynite is forming particularly in a reducing atmosphere; two different fabrics are represented for this range, with and without maghemite (d). The number of samples per mineral fabric compared against the total amount of 40 samples is included. Mineral abbreviations after Whitney and Evans [55]: Cal (Calcite), Illt (Illite), Kfs (Potassium feldspar), (Mgh) Maghemite, Ms (Muscovite), Pl (Plagioclase) and Qz (Quartz).

The general range of firing temperatures is apparently wide, though very few samples are included in the low temperature group (<750 °C). Samples fired at a temperature between 800–850 °C are the most common in this dataset and among the medieval greyware production as well [3]. Our previous research on the kiln site in Cabrera d’Anoia (Barcelona, Spain) [56] and other production areas has suggested a thorough quality control at this site, where only the pots fired at this precise temperature were exported, whereas other areas of production in Catalonia would have developed more permissive practices [3]. Pots fired between 800–850 °C have moderate strength and high toughness due to their well-sintered, but non-vitrified, clay matrix. Comparable pots fired to a lower temperature would have been weaker to withstand everyday use, and those fired to the point of vitrification would have been too brittle and easily broken. Notwithstanding this fact, pots fired at higher temperatures (900 °C and above) are also frequent in the archaeological record, which is useful for our purpose of documenting biotite breakdown.

The samples selected in this paper are representative of a wide territory in Catalonia, and hence the biotite inclusions within them have been characterized with the purpose of documenting the visual outcome of temperature affection. A wider assemblage from the kiln site of Cabrera d’Anoia has been studied under the same methodological parameters—microscopic observation and description of biotite inclusions after XRD characterization and firing temperature estimation—and has been used for comparison, even though its territorial representativeness is limited. Details about this comparison dataset are offered in Appendix B. Further remarks on XRD analysis and discussion about these materials have been published in our previous research outcomes [3].

3.2. Characterization of Biotite Inclusions

Table 1 provides a description of the biotite inclusions in medieval greyware pottery samples analysed in this paper according to the estimated firing temperature from XRD results. The colour and optical activity of the clay matrix have been recorded as well, in order to correlate the optical transformation of the paste with those specific alterations of biotite. All the thin-sections studied are vertical cuts along the vessel generatrix and perpendicular to the rim plane. Due to the common alignment of tabular inclusions in parallel to the vessel walls due to wheel-throwing, in most cases biotite inclusions show elongate or needle-like shapes.

Table 1. Details of the 40 medieval greyware pottery samples analysed in this paper, including their mineralogical assemblages as determined by XRD, the colour and optical activity of their matrices observed in thin-sections under crossed polars, their estimated firing temperature and the optical properties of the biotite inclusions contained within them.

Sample Slide ID	Mineral Assemblage ¹ (XRD)	Clay Matrix		Estimated Temperature	Biotite Features				
		Colour	Optical Activity		Colour	Size (mm)	Shape	Pleochroism	Cleavage
SMVa06	Ilt-Ms-Cal-Qz-Pl	Grey to dark brown	Moderate to high	<750 °C	Dark brown	0.5	Elongate	Weak	Normal
SMVa09	Ilt-Cal-Qz	Grey to dark brown	Moderate to low	<750 °C	Dark brown	0.5	Needle-like	Weak	Normal
SUL14	Ilt-Ms-Cal-Qz-Pl-Kfs	Greyish brown	Moderate to high	<750 °C	Red to brown	<0.25	Needle-like	Moderate	Normal
TMO02	Ilt-Qz-Pl-Kfs	Reddish to dark brown	Moderate	800–850 °C	Pale brown	0.25–0.5	Needle-like	Moderate to Weak	Normal
CTM02	Ilt-Qz-Pl-Kfs	Grey to black	Very low	800–850 °C	Pale to dark brown	0.5–1	Elongate	Moderate	Normal
SPM05	Ilt-Qz-Pl-Kfs	Reddish to dark brown	Moderate to low	800–850 °C	Red to pale brown	0.5–1	Elongate	Moderate to strong	Normal
CB07	Ilt-Qz-Pl-Kfs	Dark brown	Moderate to low	800–850 °C	Red to brown	0.5–1	Elongate	Moderate to strong	Normal
SMV14	Ilt-Qz-Pl-Kfs	Dark brown	Moderate to low	800–850 °C	Dark brown	0.5	Elongate	Weak	Normal
SUL38	Ilt-Qz-Pl-Kfs	Grey	Low	800–850 °C	Dark brown	0.5	Elongate	Weak	Normal to open
CAU22	Ilt-Qz-Pl-Kfs	Reddish to dark brown	Moderate	800–850 °C	Red to pale brown	0.5	Elongate	Strong	Normal
CAU29	Ilt-Qz-Pl-Kfs	Orange to pale brown	Moderate to high	800–850 °C	Dark brown	<0.25	Needle-like	Moderate	Normal
CAU36	Ilt-Qz-Pl-Kfs	Pale brown	Moderate	800–850 °C	Red to pale brown	0.25–0.5	Elongate	Strong to very strong	Normal to open
CAU25	Ilt-Qz-Pl-Kfs	Dark brown	Low	800–850 °C	Dark brown	0.25–1	Elongate	Very weak to none	Normal
SFG16	Ilt-Qz-Pl-Kfs	Orange to pale brown	Moderate to low	800–850 °C	Pale to dark brown	0.25–0.5	Needle-like	Moderate	Normal to open
SFG10	Ilt-Qz-Pl-Kfs	Greyish brown	Moderate	800–850 °C	Dark brown	0.5	Elongate	Weak	Normal to open
SAO18	Ilt-Qz-Pl-Kfs	Orange to pale brown	Moderate	800–850 °C	Pale to dark brown	0.25–1	Elongate	Weak	Open
E32	Ilt-Qz-Pl-Kfs	Reddish to dark brown	Low	800–850 °C	Dark brown	0.25	Elongate	Very weak	Normal
E27	Ilt-Qz-Pl-Kfs	Orange to pale brown	Moderate	800–850 °C	Red to dark brown	<0.25	Needle-like	Weak	Normal
E42	Ilt-Qz-Pl-Kfs	Orange to pale brown	Moderate	800–850 °C	Red to dark brown	0.25–0.5	Elongate	Weak	Normal to open
SAO03	Ilt-Ab/An-Qz-Pl-Kfs	Orange to pale brown	Low	900 °C	Red to dark brown	0.25	Needle-like	Moderate	Normal to open
SAO04	Ilt-Ab/An-Qz-Pl-Kfs	Reddish to dark brown	Very Low	900 °C	Dark brown	0.5	Elongate	Weak	Open
SAO10	Ilt-Ab/An-Qz-Pl-Kfs	Dark brown to black	Low to none	900 °C	Red to dark brown	0.25–0.5	Elongate	Weak	Normal to open
SMV33	Ilt-Qz-Pl-Kfs-Mgh	Reddish to dark brown	Low	900–950 °C	Very dark brown	0.25–0.5	Elongate	Weak to none	Normal to open
SJS04	Ilt-Qz-Pl-Kfs-Mgh	Orange to pale brown	Moderate to low	900–950 °C	Very dark brown	<0.25	Needle-like	Weak to none	Normal to open
SJA04	Ilt-Qz-Pl-Kfs-Mgh	Very dark brown	Low to none	900–950 °C	Red to dark brown	0.5	Elongate	Weak	Normal
CR14	Qz-Pl-Kfs-Mgh	Grey to black	None	900–950 °C	Red to dark brown	0.25–0.5	Elongate	Weak	Normal to open
CB04	Qz-Pl-Kfs-Mgh	Grey to black	Very low to none	900–950 °C	Very dark brown	0.25–1	Elongate	Weak to none	Open
CB03	Qz-Pl-Kfs	Grey to black	None	900–950 °C	Dark brown	0.5–1	Elongate	Weak to none	Open
SCO02	Qz-Pl-Kfs	Grey	Very low to none	900–950 °C	Very dark brown	0.5–1	Elongate	Weak to none	Open
CR02	Qz-Pl-Kfs-Hc	Dark brown	None	>950 °C	Pale to dark brown	0.5–1	Elongate	None	Very open
GAV01	Qz-Pl-Kfs-Hc	Dark grey	None	>950 °C	Dark brown	0.25–0.5	Needle-like	None	Open to very open
SPM20	Qz-Pl-Kfs-Hc	Dark brown to black	None	>950 °C	Pale to dark brown	0.5–1	Elongate	Very weak to none	Open
TSA01	Qz-Pl-Kfs-Hc	Dark grey to black	None	>950 °C	Dark brown to black	0.5–1	Elongate	None	Open to very open
SPM02	Qz-Pl-Kfs-Hc	Dark grey to black	None	>950 °C	Dark brown	<0.25	Elongate	None	Normal to open
SMVa02	Qz-Pl-Kfs-Hc	Dark brown to black	None	>950 °C	Very dark brown	<0.25	Elongate	None	Normal
ViB13	Qz-Pl-Kfs-Hc	Dark brown to black	None	>950 °C	Dark brown to black	0.25–0.5	Elongate	None	Normal to open
ViB04/05	Qz-Pl-Kfs-Hc	Very dark brown	None	>950 °C	Red to dark brown	0.25	Elongate	None	Normal to open
CAU26	Qz-Pl-Kfs-Hc	Black	None	>950 °C	Very dark brown	0.25–0.5	Elongate	None	Vitrified
E38	Qz-Pl-Kfs-Hc	Dark brown to black	None	>950 °C	Dark brown to black	<0.25	Needle-like	None	Normal to open
SMV34	Ab-Qz-Pl-Hc-Mgh	Dark brown to black	None	>950 °C	Black	0.5–1	Elongate	None	Open

¹ Mineral abbreviations after Whitney and Evans [55]: Illite (Ilt), Muscovite (Ms), Calcite (Cal), Quartz (Qz), Plagioclase (Pl), Potassium Feldspar (Kfs), Albite (Ab); Anorthite (An), Maghemite (Mgh) and Hercynite (Hc).

At the lowest temperature, and therefore potentially closer to their original aspect, biotite inclusions are euhedral to subhedral, tabular, fresh, pale-to-reddish or dark brown and well-cleaved, as shown in Figure 4. Cleavage is described as ‘normal’, when it is properly identifiable but the inclusions keep tight together and do not separate along the cleavage planes. This separation is a common effect of temperature [23] (p. 191), and when it is detected we estimate its degree by defining it as ‘normal to open’, ‘open’ or ‘very open.’ Most of the inclusions are 0.25–0.5 mm in size, occasionally smaller (<0.25 mm) and rarely larger (1 mm). Even though biotite pleochroism is expected to be strong, this is not a common feature in our dataset, plausibly due to the effects of firing.

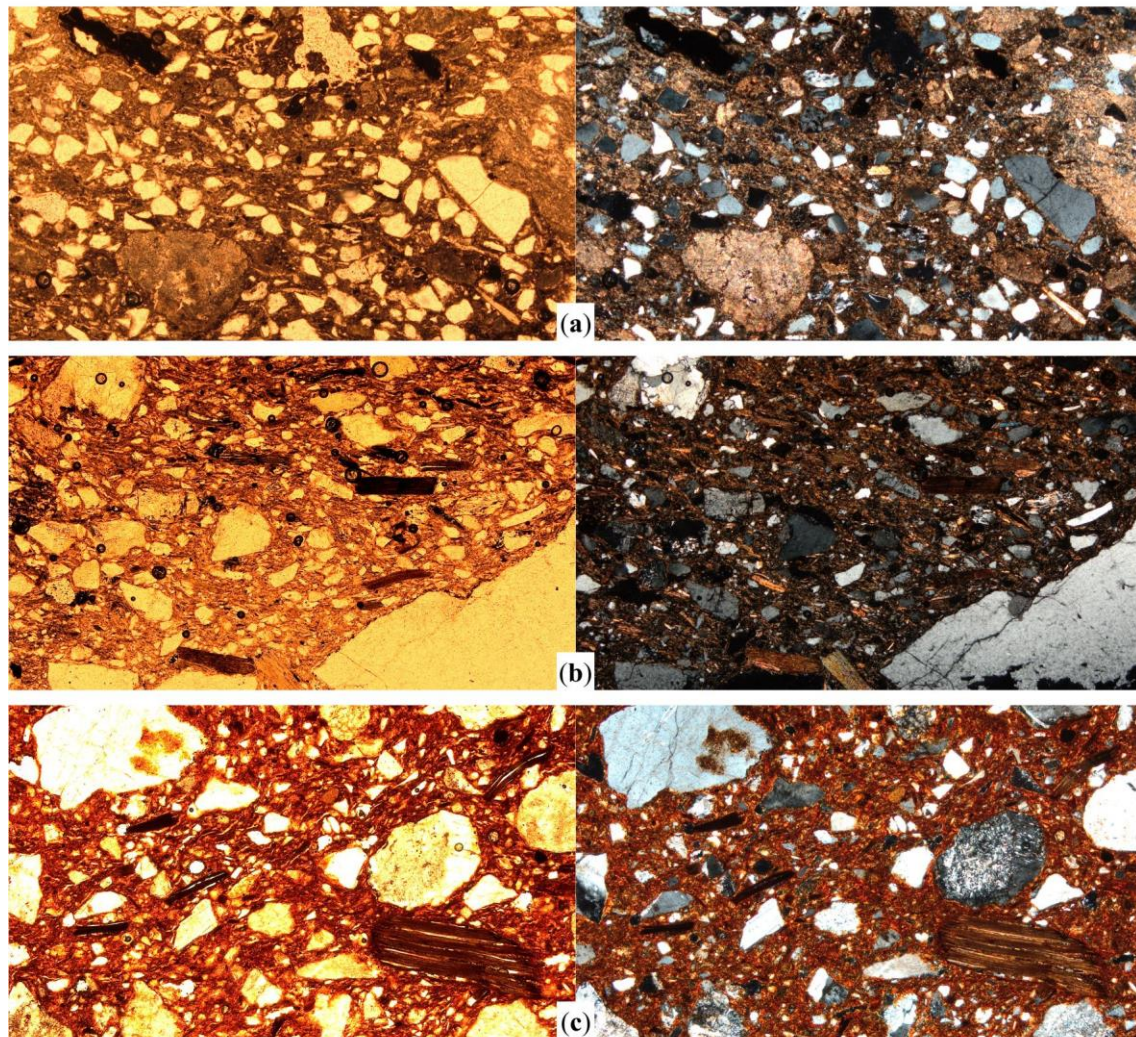


Figure 4. Photomicrographs of the selected samples with an estimated range of firing temperatures below 900 °C showing the main features of biotite inclusions. Sample SMVa06, with limestone inclusions, fired below 750 °C (a); sample SPM05 with moderate to highly pleochroic biotite fired at 800–850 °C (b); and sample SAO04, fired at about 900 °C with slightly open cleavage in biotite inclusions (c). All the images were captured in plane polarized light (left column) and crossed polars (right column), at 40× magnification. Image width = 3 mm.

The shape (elongate or needle-like) of the inclusions does not have any correlation—positive or negative—with the pleochroism shown at this stage. This optical phenomenon has also been compared to the colour and optical activity of the clay matrix [23] (pp. 93–97), which is expected to lose its birefringence at 800–850 °C. The results are particularly interesting for the range 800–850 °C. Different examples are shown in Figure 5.

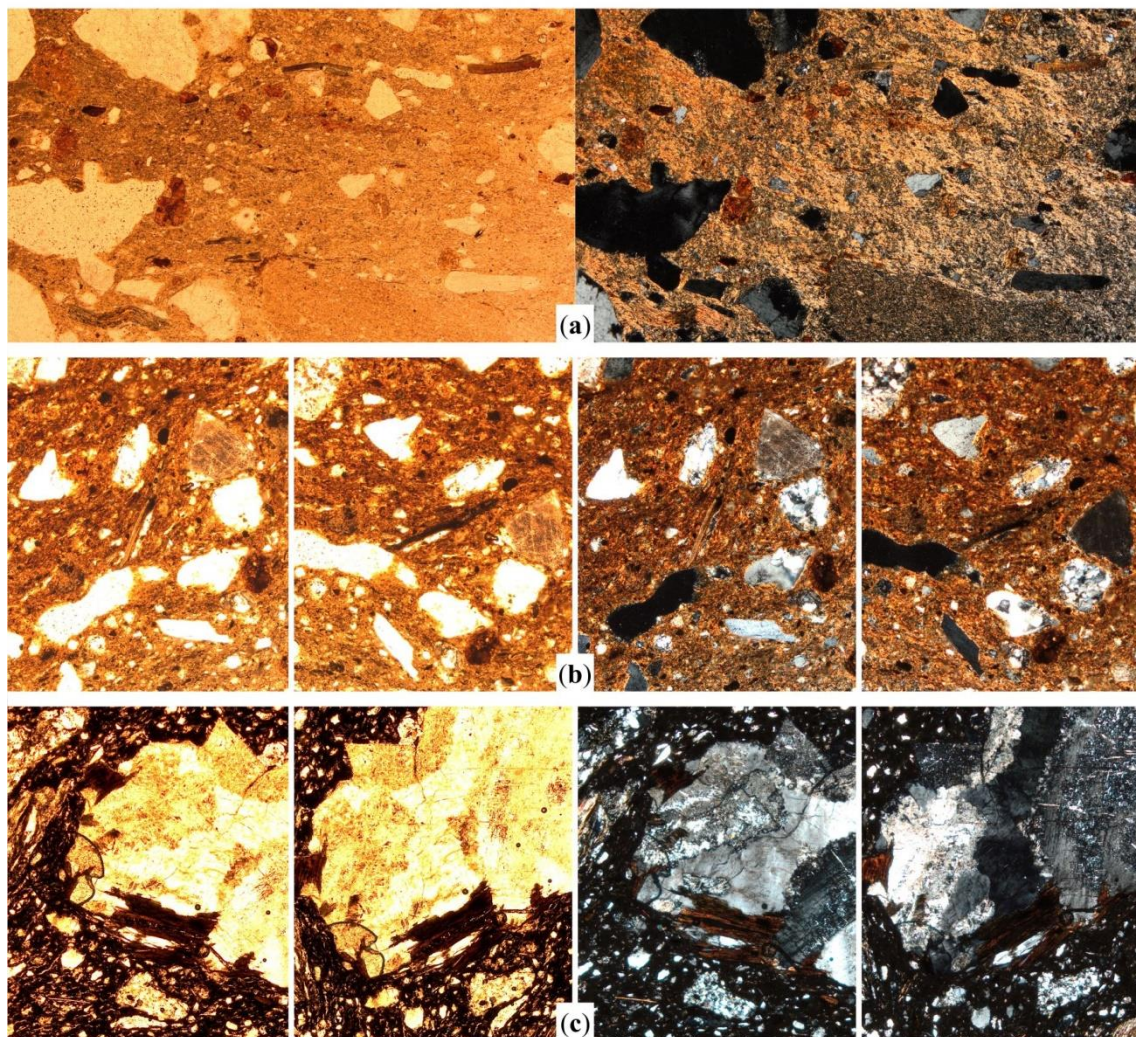


Figure 5. Photomicrographs of specific features of biotite inclusions in some selected samples fired within a range between 800–850 °C. Sample CAU36 shows high to very high pleochroism of biotite related to a moderate birefringence of clay matrix (a); samples SFG16 (b) and CTM02 (c) are shown at different rotation degrees in order to highlight the loss of pleochroism and colour darkening. All the images were captured in plane polarized light (left column) and crossed polars (right column), at 40× magnification. Image width = 3 mm [1.5 mm in (b) and (c)].

There is a certain correlation between matrix birefringence and biotite pleochroism within samples fired between 800–850 °C (Figure 5a). This phenomenon is particularly observable in more oxidized samples. Partial or incomplete reduction of the clay matrix results into an orange or reddish to pale brown colour. These samples frequently show matrices with moderate to low birefringence and moderate or moderate to strong pleochroism in biotite (Figure 5b). As matrices become more anisotropic, biotite inclusions lose pleochroism and their colour turns progressively to dark brown. This phenomenon can be observed both in isolated biotite inclusions and in biotite crystals within rock fragments—usually granitic—contained among the non-plastic inclusions assemblage (Figure 5c).

Above 900 °C biotite inclusions exhibit significant alteration well-correlated with the optical features of the matrix. Figure 6 shows some examples of biotite alteration at this range of temperatures. In most of the examined samples classified within the specific range between 900–950 °C, matrices are dark brown or grey to black without any optical activity or, rarely, very low. Biotite pleochroism in these samples is low to none (see Table 1) and colour is particularly dark (Figure 6a). Cleavage below 950 °C is still normal in some samples, but normal to open in some others, as shown in the selected example in Figure 6a,

where some biotite inclusions—see the biotite inclusion at the bottom left corner of the picture—begin to separate along their cleavage plans.

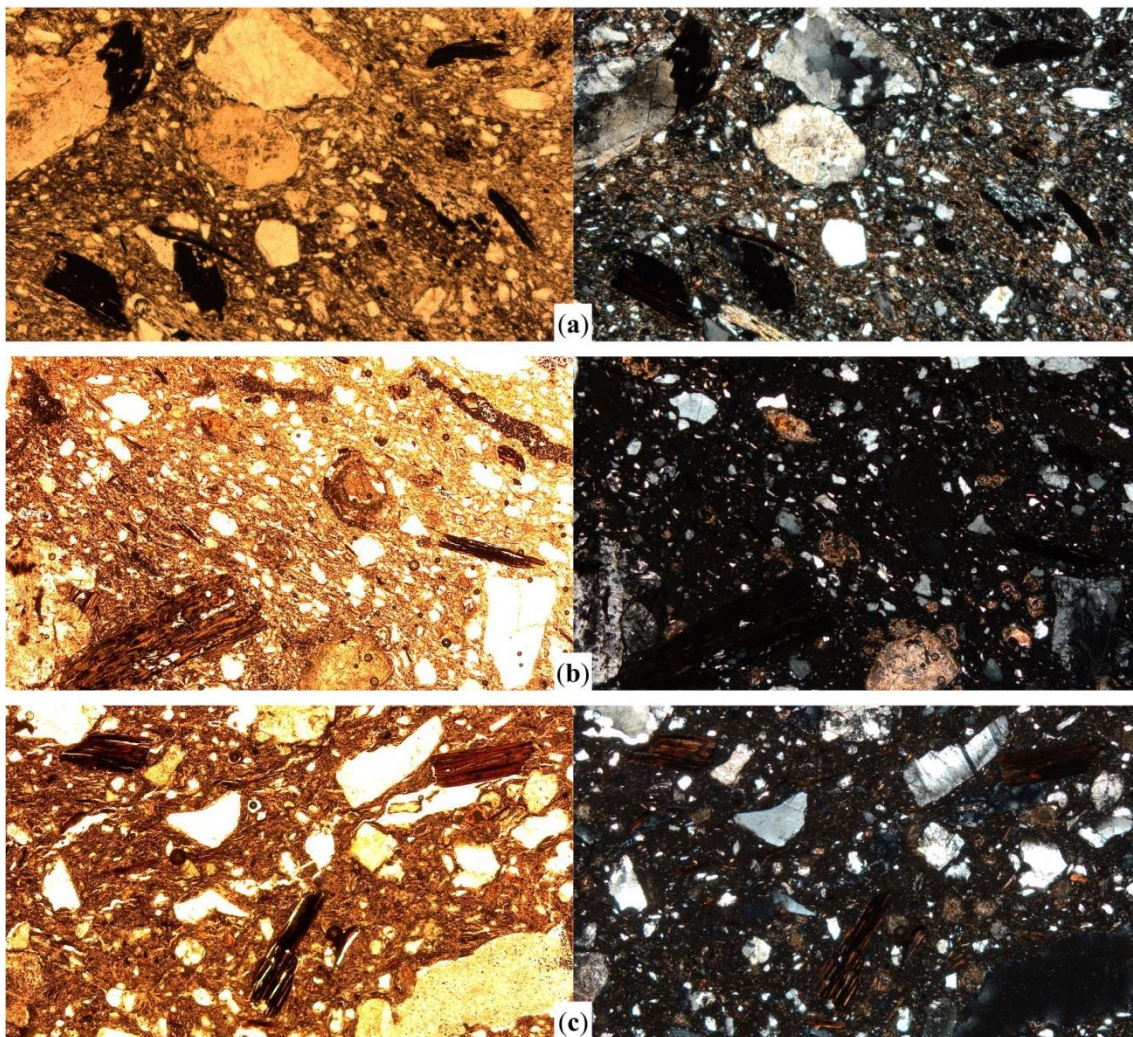


Figure 6. Photomicrographs of the selected samples with an estimated range of firing temperatures above 900 °C showing the main features of biotite inclusions. Sample SCO02 has an estimated temperature range of 900–950 °C, and shows moderately open cleavage in biotite and low pleochroism (a); samples SPM20 (b) and CR02 (c) were fired above 950 °C and show more altered features in biotite. All the images were captured in plane polarized light (left column) and crossed polars (right column), at 40× magnification. Image width = 3 mm.

When firing temperature reaches >950 °C, biotite alteration is obvious in most of the samples analysed. The birefringence of the matrix is completely absent, and pleochroism of biotite is also very weak. Even when biotite has not darkened completely and remains pale to reddish brown occasionally (Figure 6b), pleochroism is almost non-existent in many inclusions. Open cleavage is predominant and sometimes very open (Figure 6c). Regarding their shape, it should be highlighted that elongated inclusions with considerable size (≥ 0.5 mm) are frequent and needle-like smaller inclusions are not so common. This suggests that more exfoliated biotites suffer more intensely the effects of temperature, since they are thinner and have more of their surface in contact with the heat. As shown in lower temperature ranges, they lose their pleochroism earlier and, at a higher temperature phase, it could be presumed that most of them disappear.

At temperatures >950 °C other effects might be observable. The outcome of overfiring is self-evident in sample CAU26 (Figure 7a). Many of the inclusions in this sample had almost disappeared; and the clay matrix exceeded the vitrification point and shows a

'bloating' microstructure visible under plane polarized light and complete anisotropy under crossed polars. In this case, biotite inclusions were affected by overfiring as well and became part of the same vitrified microstructure. In addition to biotite alteration and clay matrix sintering (or subsequent vitrification), other effects of temperature can be detected in other minerals. Figure 7b shows a slightly altered amphibole (hornblende) inclusion, showing a brownish absorption colour instead of proper green. This is an effect estimated to happen at c. 750 °C [23] (p. 191), and this sample reached a higher temperature (800–850 °C).

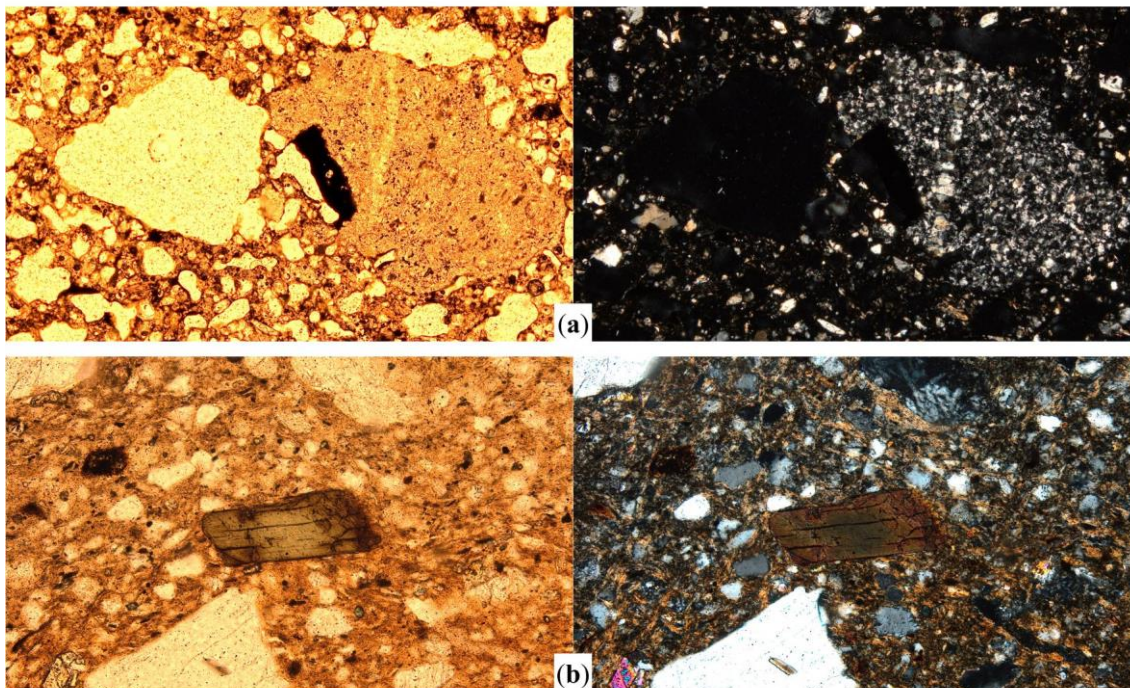


Figure 7. Photomicrographs of high temperature sample CAU26 (a), showing vitrified matrix and a biotite inclusion; and hornblende inclusion in sample SAO18 (b) with colour and optical properties slightly altered by heat. All the images were captured in plane polarized light (left column) and crossed polars (right column). Sample CAU26 (a) is pictured at 40× magnification. Image width = 3 mm. Sample SAO18 (b) is pictured at 100× magnification. Image width = 1 mm.

Amphibole inclusions being rare or very rare among the medieval greyware thin-section assemblage, it is difficult to get any further on the characterization of these minerals. Here, I just outline the value of the petrographic approach and its potential to address specific topics of ceramic technology related to colour and optical behaviour, as will be discussed in the section below.

4. Discussion

Determining the temperature effect on the biotite structure and appearance is difficult because of complications arising from the multiple oxidation states of the iron and from dehydroxylation–oxidation reactions [42] (p. 519). Geological literature on this topic investigates the significant variation of the structural parameters of biotite under high-temperature and high-pressure conditions, which are the typical variables in metamorphic contexts. Pressure does not seem to be a determinant factor for mineral transformation in pottery production processes, but firing temperature somehow reproduces this structural transformation environment. Notwithstanding this complexity, our research is focused on pottery fired under reducing atmosphere in all cases, with firing structures and conditions very similar in most of the archaeological sites known in Catalonia. Therefore, the transformations of biotite explored throughout this paper are explanatory for this specific kind of earthenware and might be a useful for comparison with other pottery thin-section studies.

In order to explore these changes, we recorded biotite's features according to the temperature ranges previously examined via XRD. We interpreted the mineralogical differences between samples in terms of firing temperature. It could be suggested that other factors like natural variability in the clays might be the reason for mineralogical differences; but bulk chemistry exploration of these samples demonstrate that the same chemical groups.

The transformations related to biotite destabilization are suggested to begin at temperatures c. 750–800 °C [34,35,39] and continue at higher temperatures [57], when thermal dehydroxylation occurs (900–1225 °C) [58] (p. 2798). As these are the most common temperature ranges in the firing of greywares, it is possible to identify and discuss specific changes in biotite inclusions and to use them as thermal or technological markers of firing technology in ceramic petrography.

Biotite (ideal formula $[K(Mg,Fe)_3(Si_2Al)O_{10}(OH)_2]$) is a 2:1 phyllosilicate mineral with tightly held, non-hydrated interlayer cations. The 2:1 layer has octahedrally coordinated cations sandwiched between two sheets of silica and alumina tetrahedra. The main cations in the octahedral layer are magnesium and divalent iron (Fe^{2+}), and the interlayer ion is mainly potassium (K^+). As suggested in [32] (p. 3793), an expansion of the interlayer regions due to an exchange of non-hydrated K^+ for hydrated or hydrolysed ions, with subsequent curling of the layers, might occur under hyper-alkaline conditions. However, interlayer K depletion is a very common phenomenon among the transformations of biotite in weathering [27] (p. 217) or increasing-temperature contexts as well, together with hydrogen loss and concomitant oxidation of Fe^{2+} to Fe^{3+} [39,59]. These initial reactions begin at temperatures $\geq 400^\circ C$ [38] (p. 89), although the resulting transformations might not be visible yet. As shown in the results section above, interlayer K depletion in the origin of biotite laths separating along cleavages is observable in samples fired at c. 900 °C or above, and it is self-evident in most biotite inclusions in the samples above 950 °C. At a range of 800–850 °C, some samples might show this 'open-cleavage' effect depending on their size.

Certainly, particle size is relevant in the degree of alteration observable in biotite inclusions, as assessed by previous studies on this topic [58]. Chemical exchange and mineral neo-formation closely depend on mineral grain size and the modal proportion of elements involved in geochemical transformation [36] (p. 1158). This is due to the larger extension of the fast-dissolving surface area in contact with heat or other destabilization agents [33] (p. 377). Our observation of biotite in pottery thin-sections suggests that assessing the effects of firing in >0.5-mm-sized inclusions might be more suitable for temperature estimation. At this size, most of the inclusions exhibit the optical affectations of heat in losing their pleochroism and showing open cleavage, but laths separation along cleavages starts significantly earlier in inclusions below this size, and needle-like inclusions of just one or two laths thin-sectioned in perpendicular will not show this effect properly if they are very small.

Iron oxidation processes also affect the appearance of biotite inclusions under the microscope, particularly related to colour and pleochroism. In non-calcareous samples fired in reducing atmosphere (as those of medieval greyware), part of the ferrous iron produced after dissociation of the iron oxides is dissolved in the vitreous matrix, and the remaining is incorporated in the spinel mineral hercynite. This reaction provides evidence for strongly reducing conditions obtained inside the clay body [60] (p. 781). Hercynite mineral is present in higher temperature samples of the studied assemblage according to the XRD results, even though it is not visible through optical microscopy examination. Nevertheless, the effect of iron alteration in reducing firing is observable in biotite darkening and pleochroism loss, which is one of the first optical indicators of biotite alteration [29,30]. It occurs along and parallel to cleavage and at biotite inclusion boundaries, and is observable in most of the samples analysed at temperatures above 800 °C. Other optical effects might be the presence of iron stained 'haloes' appearing around weathered biotite inclusions, suggesting iron release according to geological literature [27] (p. 211), but such phenomena have not been detected in our pottery samples.

5. Conclusions

Actually, there is still little literature on the archaeological domain of ceramic petrography about the visible effects of pyro-technology on pottery samples under the microscope, compared to other technological aspects such as paste preparation practices (tempering or clay mixing), or shaping methods. The decrease in optical activity of the clay matrix is one of the most used features in order to estimate firing temperatures, together with the specific transformation of some minerals. This paper is aimed at contributing to the research about the firing effects on pottery by establishing a proper record about biotite transformation at determined temperature ranges and its optical effect, but there is still significant work to be done with regard to other indicative minerals. Having a detailed record of amphibole transformation in colour or texture will also be useful to delve into the effects of firing. This is something we could sense from our dataset, but amphiboles were rare minerals within the greyware pottery assemblage studied and just a few inclusions of hornblende were examined. The results obtained were coherent with the general interpretation discussed above, but further investigation is required regarding this topic.

Obtaining this genuine grey colour in medieval and modern greyware pottery by means of reducing firing process is a specific skill transmitted from one generation of potters to another. Potters were able either to create a well-controlled oxygen-free atmosphere or, in the frequent event of using perishable or precarious firing structures, to develop strategies of quality control in order to ensure the suitability and adequacy of their products. A temperature range between 800–950 °C was frequent in medieval Catalonia, and firing temperatures were slightly higher from the 16th century onwards. Our study suggests that ceramic petrography is useful as a first-resource technique to get the bulk picture of large ceramic assemblages—including parameters related to firing technology and temperature estimation—in order to produce smaller and properly sampled assemblages for further examination of specific aspects, by means of geochemical and mineralogical techniques usually requiring higher financial effort. Pottery sherds wasted after misfiring, for instance, are easily identifiable by means of ceramic petrography and even visually with on hand specimens. Such samples might or might not be considered in further characterization studies, according to the researchers' work hypotheses or particular interests.

Therefore, counting on different elements properly documented in assessing specific issues of the technological processes in pottery is a valuable resource for archaeological research. This is the case of biotite, as we attempted to summarize throughout this paper. Biotite visual outcome of chemical and physical transformation due to firing conditions is observable at firing temperatures >800 °C, when pleochroism changes decreasingly from reddish to dark brown until pale brown to dark or anisotropic. At temperatures between 800–850 °C, biotite laths start separating as a result of interlayer K depletion, and the effect of open-cleavage is visible in some of the inclusions, particularly the smaller ones. At c. 900 °C or above, this effect is clear in most samples, together with significant darkening and total loss of pleochroism above 950 °C. Exploring these features in pottery thin-sections together with other visual alterations, such as the pleochroism of amphiboles and clay matrix optical activity, contributes to determining better sampling strategies for further examination of ceramic pyro-technology.

Funding: This paper is an outcome of the GREYWARE research project (grant number PID2019-103896RJ-I00) funded by the Spanish Ministry of Science and Innovation (MCIN—Ministerio de Ciencia e Innovación). Research was initially funded by the Catalan Government (AGAUR—Generalitat de Catalunya), as part of a collaborative project between the University of Barcelona and the University College London (Institute of Archaeology), grant number 2010-BPA-00335.

Data Availability Statement: Data supporting reported results are provided in tables and figures within the main text. Original thin-sections are kept at the Medieval and Postmedieval Archaeology Research Group GRAMP-UB at the University of Barcelona. They can be made available for researchers upon request. Additional data have been published in [1–3].

Acknowledgments: This study is part of the current research tasks carried out by the Medieval and Postmedieval Archaeology Research Group GRAMP.-UB (2017-SGR-833-GRC) at the University of Barcelona, to which the author belongs, and it is included in our Pottery Analysis research line. The author wishes to thank Noemí Travé for language edition and review. Patrick S. Quinn was supervisor of the first project (2010-BPA-00335) and kindly provided guidance and support. Colleagues at the Centre d'Estudis Martorellencs (Martorell, Barcelona) and the Archaeological Museum of l'Esquerda (Roda de Ter, Osona) provided pottery samples for analysis. The author acknowledges their cooperation. Jaume Buxeda and Marisol Madrid, to whom we acknowledge their contribution, performed XRD analyses of additional samples in Appendix B. Joan Vicens Tarré made the traditional greyware collection of Quart shown in Figure 1 available for research purposes and provided useful references on actual or sub-actual pottery production. His contribution is warmly appreciated.

Conflicts of Interest: The author declares no conflict of interest. The funders had no role in the design of the study; in the collection, analyses, or interpretation of data; in the writing of the manuscript, or in the decision to publish the results.

Appendix A

Archaeological and contextual data for samples examined in this paper are provided in Table A1 below.

Table A1. Details of the archaeological context for the 40 medieval greyware pottery samples analysed in this paper, including their site of origin and location, chronology, petrographic fabric, vessel shape, fragment and interpreted production location. Samples keep the same order as in Table 1.

Sample Slide ID	Site	Site Description	Site Location (Town)	Period (Cent. A.D.)	Petrographic Fabric	Vessel Shape	Fragment	Interpreted Production Location
SMVa06	Castelló Sobirà de Sant Gervàs	Castle	Sant Miquel de la Vall	11–14th	Coarse Quartz and Sandy Marl	Boiling pot 'olla'	Wall	Verdú
SMVa09	Castelló Sobirà de Sant Gervàs	Castle	Sant Miquel de la Vall	11–14th	Calcite, Opaques and Fine Quartz	Boiling pot 'olla'	Wall	Pyrenean Area
SUL14	Sant Sebastià del Sull	Monastery	Saldes	11–12th	Fine Quartz, Altered Feldspar and Rock Fragments	Boiling pot 'olla'	Wall	Casampons (Phase B)
TMO02	Torre del Moro	Castle	Castellfollit del Boix Santa	10–11th	Coarse Metamorphic	Boiling pot 'olla'	Wall	Probably Piera
CTM02	Camp de la Torra	Village	Margarida de Montbui	12th	Coarse Metamorphic	Boiling pot 'olla'	Wall	Probably Piera
SPM05	Collet de Sant Pere Màrtir	Necropolis	Òdena	11–13th	Coarse Metamorphic	Boiling pot 'olla'	Decorated wall	Probably Piera
CB07	Castell de Boixadors	Castle	Sant Pere Sallavinera	11–13th	Coarse Granite and Fine Quartz	Boiling pot 'olla'	Wall	
SMV14	Església de Sant Miquel	Church	Veciana	13–14th	Coarse Quartz and Sandy Marl	Boiling pot 'olla'	Wall	Verdú
SUL38	Sant Sebastià del Sull	Monastery	Saldes	11–12th	Coarse Quartz, Altered Feldspar and Rock Fragments	Boiling pot 'olla'	Wall	
CAU22	Sant Esteve de Caulers	Village	Caldes de Malavella	12–14th	Coarse Quartz and Feldspar	Boiling pot 'olla'	Base	
CAU29	Sant Esteve de Caulers	Village	Caldes de Malavella	12–14th	Coarse Quartz and Feldspar	Boiling pot 'olla'	Wall	
CAU36	Sant Esteve de Caulers	Village	Caldes de Malavella	12–14th	Coarse Sand (1)	Boiling pot 'olla'	Wall	Quart
CAU25	Sant Esteve de Caulers	Village	Caldes de Malavella	12–14th	Coarse Sand (2)	Boiling pot 'olla'	Decorated wall	Quart
SFG16	Església de Sant Feliu	Church	Girona	15th	Coarse Sand (2)	Boiling pot 'olla'	Decorated wall	Quart
SFG10	Església de Sant Feliu	Church	Girona	15th	Calcite, Opaques and Fine Quartz	Boiling pot 'olla'	Wall	Pyrenean Area
SAO18	Església de Sant Andreu	Church Sacraria	Òrrius	13th	Acidic/Intermediate Igneous Rock Fragments	Boiling pot 'olla'	Wall	Maresme (Local)
E32	L'Esquerda	Village	Roda de Ter	12–13th	Coarse Qz-Fds Rock Fragments and Clay Pellets	Boiling pot 'olla'	Decorated wall	
E27	L'Esquerda	Village	Roda de Ter	12–13th	Coarse Qz-Fds Rock Fragments and Clay Pellets	Boiling pot 'olla'	Decorated wall	

Table A1. Cont.

Sample Slide ID	Site	Site Description	Site Location (Town)	Period (Cent. A.D.)	Petrographic Fabric	Vessel Shape	Fragment	Interpreted Production Location
E42	L'Esquerda	Village	Roda de Ter	12–13th	Fine Quartz and Acidic Igneous Rock Fragments	Boiling pot 'olla'	Shoulder	
SAO03	Església de Sant Andreu	Church <i>Sacraría</i>	Òrrius	13th	Acidic/Intermediate Igneous Rock Fragments	Boiling pot 'olla'	Rim	Maresme (Local)
SAO04	Església de Sant Andreu	Church <i>Sacraría</i>	Òrrius	13th	Acidic/Intermediate Igneous Rock Fragments	Boiling pot 'olla'	Rim	Maresme (Local)
SAO10	Església de Sant Andreu	Church <i>Sacraría</i>	Òrrius	13th	Acidic/Intermediate Igneous Rock Fragments	Boiling pot 'olla'	Rim	Maresme (Local)
SMV33	Església de Sant Miquel	Church	Veciana	13–14th	Coarse Granitic with Clay Pellets	Cover	Wall	Cabrera d'Anoia
SJS04	Sant Jaume Sesoliveres	Church	Igualada	14th	Coarse Metamorphic	Boiling pot 'olla'	Wall	Probably Piera
SJA04	Sant Julià de les Alzinetes	Church	Jorba	15th	Mica and Granite	Boiling pot 'olla'	Rim	
CR14	La Creueta	Necropolis	Cabrera d'Anoia	10–12th	Fine Granitic	Boiling pot 'olla'	Rim	Cabrera d'Anoia
CB04	Castell de Boixadors	Castle	Sant Pere Sallavinera	11–13th	Coarse Metamorphic	Boiling pot 'olla'	Wall	Probably Piera
CB03	Castell de Boixadors	Castle	Sant Pere Sallavinera	11–13th	Coarse Granitic	Boiling pot 'olla'	Wall	Cabrera d'Anoia
SCO02	Església de Santa Càndia	Church	Orpí	13–14th	Coarse Metamorphic	Boiling pot 'olla'	Decorated rim	Probably Piera
CR02	La Creueta	Necropolis	Cabrera d'Anoia	10–12th	Coarse Granitic with Calcite	Jar	Rim and spout	Cabrera d'Anoia
GAV01	Santa Maria de Gàver	Church	Estaràs	11–12th	Coarse Granitic with Calcite	Casserole	Rim	Cabrera d'Anoia
SPM20	Collet de Sant Pere Màrtir	Necropolis	Òdena	11–13th	Coarse Granitic with Calcite	Cover	Rim	Cabrera d'Anoia
TSA01	Torre d'Òdena	Castle	Òdena	12–14th	Coarse Metamorphic	Boiling pot 'olla'	Wall	Probably Piera
SPM02	Collet de Sant Pere Màrtir	Necropolis	Òdena	11–13th	Fine Quartz	Boiling pot 'olla'	Wall	
SMVa02	Castelló Sobirà de Sant Gervàs	Castle	Sant Miquel de la Vall	11–14th	Micrite and Fine Quartz	Boiling pot 'olla'	Shoulder	
ViB13	Mas B de Vilosiu	Household	Cercs	12–14th	Coarse Quartz, Altered Feldspar and Rock Fragments	Boiling pot 'olla'	Base	Casampons (Phase A)
ViB04/05	Mas B de Vilosiu	Household	Cercs	12–14th	Coarse Quartz, Altered Feldspar and Rock Fragments	Boiling pot 'olla'	Wall	Casampons (Phase A)
CAU26	Sant Esteve de Caulers	Village	Caldes de Malavella	12–14th	Fine Quartz, Feldspar and Clay Pellets	Large Basin (<i>Cossi</i>)	Rim	
E38	L'Esquerda	Village	Roda de Ter	12–13th	Fine Quartz and Arkose	Boiling pot 'olla'	Shoulder	
SMV34	Església de Sant Miquel	Church	Veciana	13–14th	Fine Clay with Clay Pellets and Sandy Marl	Water jug	Wall	Verdú (late period)

Appendix B

In this appendix, we provide details on the biotite features observed in the greyware pottery thin-sections from the kiln site of Cabrera d'Anoia (Barcelona, Spain) [56]. Data summarized in Table A2 are a good complement for the representative Catalonian pottery assemblage selected for this paper, even though they are all from the same site. XRD analysis of these samples was performed at the Scientific and Technological Centres of the University of Barcelona (CCiTUB) using a Siemens D-500 X-ray diffractometer. Small subsamples (about 1 g) from each sherd were ground to a fine powder and dried at 110 °C for 12 h after the removal of the surface layer with a tungsten carbide drill. The powdered samples were spread and flattened on a standard XRD well slide and bombarded with Cu- α -radiation ($\lambda = 1.5406 \text{ \AA}$) with a graphite diffracted beam monochromator and a power of 1.2kW (40 kV, 30 mA). The diffracted X-rays were measured in the range 4.0–70.0° using 0.05° step width, a speed of 1.0°/min in continuous scanning mode. The resulting diffractograms were analysed following the same procedure as the core assemblage of samples analysed in this paper, as detailed in Section 2. Table A2 includes biotite optical description

for 100 samples from Cabrera d’Anoia. Samples are classified according to 12 fabrics with specific mineral assemblages that allow us to estimate their firing temperature range.

Table A2. Details of 100 medieval greyware pottery wasters analysed from Cabrera d’Anoia in previous research [3], including their mineralogical assemblages as determined by XRD, the colour and optical activity in thin-sections under crossed polars, their estimated firing temperature and the optical properties of the biotite inclusions contained within. Please see [56] (pp. 402–403) for petrographic fabric and geochemical group ascription and [3,56] for further details.

Sample Slide ID	Mineral Assemblage ¹ (XRD)	Clay Matrix		Estimated Temperature	Biotite Features				
		Colour	Optical Activity		Colour	Size (mm)	Shape	Pleochroism	Cleavage
CA002	Fabric 1	Dark grey	Low	<750 °C	Dark brown	0.5–1	Elongate	Low	Normal to open
CA027	Fabric 1	Pale brown	Moderate	<750 °C	Pale to dark brown	0.25–1	Elongate	Strong	Normal
CA050	Fabric 1	Reddish brown	Moderate	<750 °C	Pale to reddish brown	0.25–1	Elongate	Very strong	Normal
CA056	Fabric 1	Reddish brown	Moderate	<750 °C	Pale to dark brown	0.25–0.5	Needle-like	Very strong	Normal to open
CA057	Fabric 1	Dark grey	Very low	<750 °C	Greenish brown to black	0.25–0.5	Needle-like	Low	Normal to open
CA060	Fabric 1	Dark grey	Moderate	<750 °C	Dark brown to black	0.25–0.5	Needle-like	Low	Normal to open
CA066	Fabric 1	Grey	Low	<750 °C	Greenish to reddish brown	0.25–1	Elongate	Very Strong	Normal
CA073	Fabric 1	Reddish brown	High	<750 °C	Greenish to reddish brown	0.25–1	Elongate	Very Strong	Normal
CA074	Fabric 1	Reddish brown	High	<750 °C	Greenish to reddish brown	0.25–1	Elongate	Very Strong	Normal
CA076	Fabric 1	Orange to pale brown	Moderate	<750 °C	Pale to dark brown	0.25–1	El. and needle-like	Strong	Normal to open
CA083	Fabric 1	Reddish brown	Moderate	<750 °C	Greenish to reddish brown	0.25–0.5	El. and needle-like	Strong	Normal to open
CA089	Fabric 1	Pale brown	Moderate	<750 °C	Greenish to reddish brown	0.25–0.5	Needle-like	Strong	Normal to open
CA100	Fabric 1	Reddish brown	Moderate	<750 °C	Red to dark brown	0.25–0.5	Needle-like	Strong	Normal to open
CA101	Fabric 1	Reddish brown	Moderate	<750 °C	Orange to pale brown	0.25–0.5	Elongate	Strong	Normal
CA102	Fabric 1	Reddish brown	Moderate	<750 °C	Red to dark brown	0.25–0.5	Needle-like	Moderate	Normal
CA005	Fabric 2	Dark brown	Moderate	<750 °C	Greenish to dark brown	0.25–1	Elongate	Strong	Normal
CA007	Fabric 2	Reddish brown	Moderate	<750 °C	Yellow to greenish brown	0.5–1	Elongate	Strong	Normal to open
CA014	Fabric 2	Reddish brown	Moderate	<750 °C	Pale to reddish brown	0.25–1	Elongate	Very strong	Normal
CA017	Fabric 2	Reddish brown	Moderate	<750 °C	Greenish to reddish brown	0.5–1	Elongate	Very strong	Normal to open
CA020	Fabric 2	Reddish brown	Moderate to high	<750 °C	Greenish to reddish brown	0.5–1	El. and needle-like	Strong	Normal to open
CA022	Fabric 2	Pale brown	Moderate	<750 °C	Pale to dark brown	0.25–1	Elongate	Moderate to strong	Normal
CA023	Fabric 2	Dark brown	Moderate	<750 °C	Greenish to reddish brown	0.25–1	Elongate	Strong	Normal to open
CA024	Fabric 2	Pale brown	Moderate	<750 °C	Reddish to dark brown	0.25–1	Needle-like	Strong	Normal
CA025	Fabric 2	Reddish brown	Moderate	<750 °C	Greenish to reddish brown	0.5–1	Elongate	Strong	Normal
CA026	Fabric 2	Pale brown	Moderate	<750 °C	Greenish to reddish brown	0.25–1	Needle-like	Very strong	Normal
CA029	Fabric 2	Reddish brown	Moderate	<750 °C	Reddish to brown	0.25–1	Elongate	Moderate to strong	Normal
CA075	Fabric 2	Orange to brown	Moderate	<750 °C	Reddish to brown	0.25–0.5	Needle-like	Very strong	Normal
CA078	Fabric 2	Reddish brown	Moderate	<750 °C	Reddish to dark brown	0.5–1	Elongate	Strong	Normal to open
CA079	Fabric 2	Reddish brown	Moderate	<750 °C	Pale to dark brown	0.25–0.5	Needle-like	Strong	Normal
CA080	Fabric 2	Reddish brown	Moderate	<750 °C	Reddish to dark brown	0.25–1	Elongate	Moderate	Normal to open
CA081	Fabric 2	Orange to brown	Moderate	<750 °C	Orange to brown	0.5–1	Elongate	Very strong	Normal
CA003	Fabric 3	Pale brown	Low	<850 °C	Reddish to dark brown	0.5–1	Elongate	Strong	Normal to open
CA009	Fabric 3	Reddish brown	Low	<850 °C	Reddish to dark brown	0.25–0.5	Elongate	Strong	Normal
CA012	Fabric 3	Pale brown	Low	<850 °C	Reddish to dark brown	0.25–0.5	Elongate	Moderate	Normal to open

Table A2. Cont.

Sample Slide ID	Mineral Assemblage ¹ (XRD)	Clay Matrix			Biotite Features				
		Colour	Optical Activity	Estimated Temperature	Colour	Size (mm)	Shape	Pleochroism	Cleavage
CA031	Fabric 3	Grey	Low	<850 °C	Reddish to dark brown	0.25–0.5	Needle-like	Moderate to weak	Normal to open
CA032	Fabric 3	Greyish brown	Low	<850 °C	Reddish to dark brown	0.25–0.5	Needle-like	Moderate to weak	Normal to open
CA036	Fabric 3	Brown	Low	<850 °C	Reddish to dark brown	0.25–0.5	Needle-like	Moderate	Normal to open
CA041	Fabric 3	Reddish brown	Low	<850 °C	Reddish to dark brown	0.25–0.5	Needle-like	Moderate	Normal to open
CA042	Fabric 3	Reddish brown	Low	<850 °C	Pale to dark brown	0.25–1	Needle-like	Moderate	Normal to open
CA048	Fabric 3	Reddish to dark brown	Low	<850 °C	Dark brown	0.25–0.5	Elongate	Moderate to weak	Normal
CA051	Fabric 3	Dark grey	Low	<850 °C	Pale to dark brown	0.25–0.5	Needle-like	Moderate	Normal to open
CA067	Fabric 3	Grey	Low	<850 °C	Pale to dark brown	0.25–0.5	Needle-like	Moderate	Normal
CA072	Fabric 3	Brown	Low	<850 °C	Greenish to pale brown	0.25–1	Needle-like	Moderate	Normal to open
CA077	Fabric 3	Reddish brown	Low	<850 °C	Orange to brown	0.25–1	Elongate	Strong	Normal
CA082	Fabric 3	Orange to pale brown	Low	<850 °C	Greenish to reddish brown	0.25–0.5	Elongate	Moderate	Normal
CA095	Fabric 3	Dark Brown	Low	<850 °C	Reddish to dark brown	0.25–0.5	Needle-like	Moderate	Normal
CA103	Fabric 3	Dark grey	Low	<850 °C	Dark brown to black	0.25–0.5	Needle-like	Moderate to weak	Normal to open
CA006	Fabric 4	Dark grey to black	None	800–900 °C	Dark brown to black	0.25–0.5	Needle-like	None	Open
CA010	Fabric 4	Brown	Very low	800–900 °C	Dark brown to black	0.25–1	Elongate	Very weak	Very open
CA011	Fabric 4	Dark grey	None	800–900 °C	Dark brown to black	0.25–0.5	Needle-like	Very weak	Open
CA013	Fabric 4	Dark grey	None	800–900 °C	Dark brown to black	0.25–1	Needle-like	Very weak	Open
CA018	Fabric 4	Dark brown	Very low	800–900 °C	Dark brown to black	0.25–0.5	El. and needle-like	Very weak	Very open
CA021	Fabric 4	Grey	None	800–900 °C	Greenish to black	<0.25	Needle-like	Very weak	Normal to open
CA028	Fabric 4	Dark brown	Very low	800–900 °C	Dark brown to black	0.25–1	Elongate	None	Open
CA062	Fabric 4	Reddish brown	Very low	800–900 °C	Reddish to brown	0.5–1	Elongate	Weak	Normal to open
CA068	Fabric 4	Brown	Very low	800–900 °C	Reddish to brown	0.25–1	Elongate	Weak	Normal
CA069	Fabric 4	Dark grey	None	800–900 °C	Dark brown to black	0.25–1	Needle-like	None	Normal to open
CA070	Fabric 4	Dark grey	Very low	800–900 °C	Dark brown to black	0.25–0.5	Needle-like	Very weak	Normal to open
CA004	Fabric 5	Reddish brown	Very low	800–950 °C	Reddish to brown	0.5–1	Elongate	Very weak	Open to very open
CA015	Fabric 5	Dark brown	Very low	800–950 °C	Dark brown to black	0.5–1	Elongate	Very weak to none	Normal to open
CA063	Fabric 5	Dark grey to black	Very low to none	800–950 °C	Dark brown to black	0.25–1	El. and needle-like	Very weak to none	Open to very open
CA091	Fabric 5	Reddish brown	Very low to none	800–950 °C	Pale to dark brown	0.5–1	Elongate	Weak	Open
CA033	Fabric 6	Dark grey	None	875–900 °C	Reddish brown to black	0.25–1	El. and needle-like	None	Open to very open
CA046	Fabric 6	Reddish brown	None	875–900 °C	Reddish to brown	0.5–1	Elongate	Very weak	Open
CA038	Fabric 7	Dark grey	None	c. 900 °C	Dark brown to black	0.25–0.5	Elongate	Weak	Open
CA039	Fabric 7	Dark grey	None	c. 900 °C	Dark brown to black	0.25–0.5	Elongate	Weak	Open
CA043	Fabric 7	Dark brown to black	None	c. 900 °C	Dark brown to black	0.25–0.5	Elongate	Very weak to none	Open to very open
CA049	Fabric 7	Dark brown to black	None	c. 900 °C	Reddish brown to black	0.25–1	Elongate	Weak	Open
CA052	Fabric 7	Dark brown to black	None	c. 900 °C	Dark brown to black	0.5–1	Elongate	Very weak to none	Open
CA054	Fabric 7	Dark brown to black	None	c. 900 °C	Reddish brown to black	0.25–0.5	Needle-like	Very weak to none	Open
CA104	Fabric 7	Dark grey	None	c. 900 °C	Reddish to dark brown	0.5–1.5	Elongate	Weak	Open to very open
CA016	Fabric 8	Black	None	>900 °C	Black	0.25–0.5	Elongate	None	Vitrified
CA084	Fabric 9	Reddish brown	None	900–950 °C	Reddish to dark brown	0.25–0.5	Elongate	Weak	Open

Table A2. Cont.

Sample Slide ID	Mineral Assemblage ¹ (XRD)	Clay Matrix			Biotite Features				
		Colour	Optical Activity	Estimated Temperature	Colour	Size (mm)	Shape	Pleochroism	Cleavage
CA085	Fabric 9	Dark brown	None	900–950 °C	Dark brown	0.25–0.5	Elongate	None	Normal to open
CA086	Fabric 9	Dark brown to black	None	900–950 °C	Dark brown to black	0.25–0.5	Elongate	None	Open to very open
CA087	Fabric 9	Black	None	900–950 °C	Dark brown to black	0.25–0.5	El. and needle-like	None	Open to very open
CA088	Fabric 9	Black	None	900–950 °C	Dark brown to black	0.25–0.5	Needle-like	Very weak to none	Open
CA001	Fabric 10	Dark brown	None	900–950 °C	Black	0.25–1	El. and needle-like	Very weak to none	Open
CA030	Fabric 10	Dark grey	None	900–950 °C	Black	0.25–0.5	Needle-like	None	Open to very open
CA071	Fabric 10	Black	None	900–950 °C	Dark brown to black	0.25–0.5	Needle-like	None	Open
CA090	Fabric 10	Black	None	900–950 °C	Dark brown to black	0.25–1.5	El. and needle-like	None	Open to very open
CA094	Fabric 10	Dark brown	None	900–950 °C	Reddish brown to black	0.25–0.5	Elongate	Very weak to none	Open
CA105	Fabric 10	Dark brown to black	None	900–950 °C	Black	0.25–0.5	Elongate	Very weak to none	Open
CA019	Fabric 11	Dark brown	None	>950 °C	Pale to dark brown	0.25–1	Elongate	None	Open
CA045	Fabric 11	Black	None	>950 °C	Black	0.25–1	Elongate	None	Open
CA034	Fabric 12	Black	None	>950 °C	Black	0.25–0.5	Needle-like	None	Open
CA037	Fabric 12	Black	None	>950 °C	Reddish brown	0.25–1	Elongate	None	Open
CA040	Fabric 12	Black	None	>950 °C	Black	0.25–0.5	Elongate	None	Very open
CA044	Fabric 12	Black	None	>950 °C	Black	0.25–0.5	Needle-like	None	Open
CA047	Fabric 12	Brown	None	>950 °C	Dark brown	0.25–0.5	Elongate	Very weak to none	Open
CA053	Fabric 12	Black	None	>950 °C	Black	0.25–0.5	El. and needle-like	None	Open
CA059	Fabric 12	Reddish brown	None	>950 °C	Reddish to dark brown	0.25–0.5	Elongate	None	Open
CA061	Fabric 12	Black	None	>950 °C	Black	0.25–0.5	Elongate	None	Open to very open
CA064	Fabric 12	Black	None	>950 °C	Black	0.25–1	Elongate	None	Open
CA065	Fabric 12	Reddish brown	None	>950 °C	Reddish to dark brown	0.25–1	Elongate	None	Normal to open
CA092	Fabric 12	Black	None	>950 °C	Black	0.25–0.5	El. and needle-like	None	Very open
CA093	Fabric 12	Black	None	>950 °C	Black	0.25–1	Elongate	None	Very open
CA099	Fabric 12	Black	None	>950 °C	Black	0.25–1	Elongate	None	Very open

¹ Mineral assemblages are summarized in fabrics as follows; (Question marks indicate the tentative presence of specific minerals): Fabric 1–Illite–Calcite–Quartz–Plagioclase–K Feldspar; Fabric 2–Illite–Muscovite–Anorthite–Calcite–Quartz–Plagioclase–K Feldspar; Fabric 3–Illite–Quartz–Plagioclase–K Feldspar; Fabric 4–Calcite–Quartz–Plagioclase–K Feldspar–Maghemite; Fabric 5–Illite–Quartz–Plagioclase–K Feldspar–Maghemite; Fabric 6–Quartz–Plagioclase–K Feldspar; Fabric 7–Quartz–Plagioclase–K Feldspar–Maghemite; Fabric 8–Quartz–Plagioclase–K Feldspar–Maghemite (*Low peak*); Fabric 9–Illite (*Low peak*)–Quartz–Plagioclase–K Feldspar–Maghemite–Hercynite? Fabric 10–Quartz–Plagioclase–K Feldspar–Maghemite–Hercynite (*Low peak*); Fabric 11–Quartz–Plagioclase–K Feldspar–Hercynite; Fabric 12–Quartz–Plagioclase–K Feldspar–Maghemite–Hercynite.

Figure A1 below illustrates biotite transformation in colour, optical properties and texture at different temperature ranges. Samples from the kiln site of Cabrera d’Anoia illustrate the loss of pleochroism, darkening in colour and cleavage opening according to the results and discussion developed in the core sections of this paper.

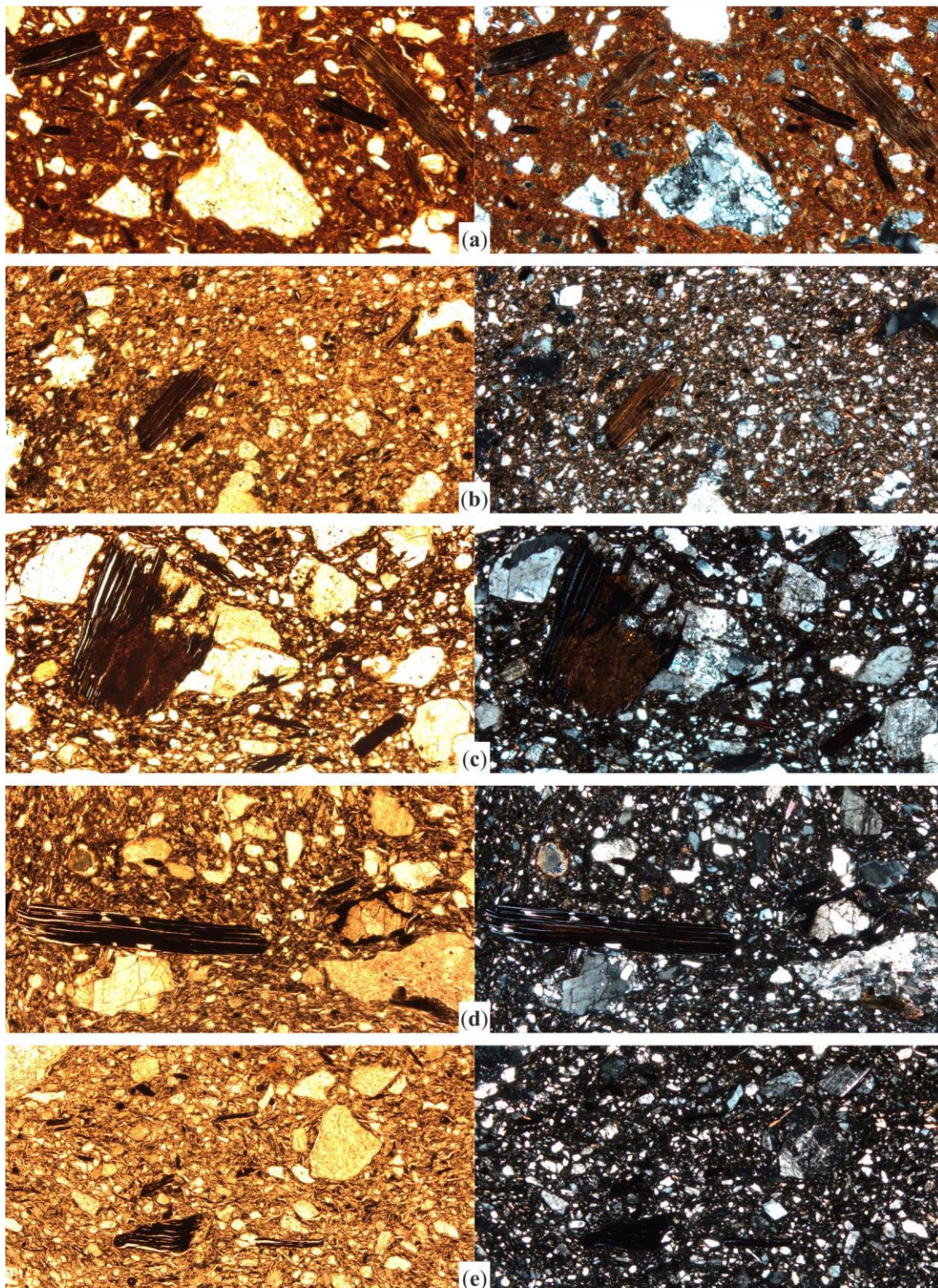


Figure A1. Photomicrographs of selected samples from Cabrera d'Anoia. Sample CA017 (a) was fired at <750 °C and shows strong pleochroism and normal cleavage in most inclusions. Sample CA031, fired at <850 °C still includes pleochroic inclusions but laths start separating (b). At 900 – 950 °C and above, cleavage is open or very open according to temperature increase, as shown in sample CA104 (c), still with weak pleochroism, and CA090 (d) with non-pleochroic dark brown inclusions. Above 950 °C, biotite inclusions are usually black under reducing atmosphere, with very open cleavage as shown in sample CA040 (e). All the images were captured in plane polarized light (left column) and crossed polars (right column), at $40\times$ magnification. Image width = 3 mm.

References

1. Travé, E.; Quinn, P.S.; López, M.D. To the vicinity and beyond! Production, distribution and trade of cooking greywares in medieval Catalonia, Spain. *Archaeol. Anthropol. Sci.* **2016**, *8*, 763–778.
2. Travé, E. *La Ceràmica Comuna de Cuina D'època Medieval: Provenença, Tecnologia i Comerç al Camp Català*, 1st ed.; Societat Catalana d'Arqueologia: Barcelona, Spain, 2018.
3. Travé, E.; Quinn, P.S.; Álvaro, K. Another one bites the dust: Firing technology and quality control in the production of medieval greyware ceramics from Catalonia, Spain. *Archaeometry* **2019**, *61*, 1280–1295. [[CrossRef](#)]
4. Picon, M.; Thiriot, J.; Abraços, H.; Diogo, J. Estudo em laboratório e observação etnoarqueológica das cerâmicas negras portuguesas. In *Actas das 1as Jornadas de Cerâmica Medieval e Pós-Medieval. Métodos e Resultados Para o Seu Estudo (1992)*, 1st ed.; Câmara Municipal de Tondela: Porto, Portugal, 1995; pp. 189–206.
5. Musty, J. Medieval Pottery Kilns. In *Medieval Pottery from Excavations*, 1st ed.; Evison Vera, I., Hodges, H., Hurst, J.G., Eds.; John Baker: London, UK, 1974; pp. 41–65.
6. Echallier, J.-C.; Montagu, J. Données quantitatives sur la préparation et la cuisson en four à bois de reconstitutions actuelles de poteries grecques et romaines [Technologies céramiques]. *Doc. d'Archéologie Méridionale* **1985**, *8*, 141–145. [[CrossRef](#)]
7. Allios, D.; Lagarrigue, P. Archéologie expérimentale des fours à bois. In *Turner Autour du Pot . . . Les Ateliers de Potiers Médiévaux du Ve au XIIIe Siècle Dans L'espace Européen*, 1st ed.; Thuillier, F., Louis, E., Eds.; Publications du CRAHAM, Presses Universitaires de Cahen: Cahen, France, 2015; pp. 642–658.
8. Hanning, E.; Döhner, G.; Grunwald, L.; Hastenteufel, A.; Rech, A.; Axtmann, A.; Bogott, A. Experimental Reconstruction and Firing of a 5/6th Century Updraft Kiln from Mayen, Germany. *Exp. Archäologie Eur.* **2016**, *15*, 60–73.
9. Amicone, S.; Rogier, M.; Berthold, C.; Kiemle, T.; Sconzo, P.; Morandi, L.; Gur-Arieh, S.; Seidler, J.; Memmesheimer, A.; Awais Qarni, M.; et al. An interdisciplinary approach to the study of kiln firing: A case study from Campus Galli. In Proceedings of the Experimental Archaeology Conference, Trento, Italy, 2–3 May 2019.
10. Casademont, L. Lluís Cornellà: Anàlisi d'un procés de fer negre. In *Miscel·lània Premis Pere Lloberas 1989 i 1990*, 1st ed.; Ajuntament de la Bisbal d'Empordà: La Bisbal d'Empordà, Spain, 1991; pp. 74–97.
11. Rocas, X. Lluís Cornellà Font y el proceso de elaboración de la alfarería negra de La Bisbal d'Empordà. In *Obra Negra y Alfarería de Cocina. Actas del XIX Congreso de la Asociación de Ceramología*, 1st ed.; Ajuntament de Quart: Quart (Girona), Spain, 2017; pp. 151–169.
12. Carreras, J. *Els Fornos Tradicionals de Ceràmica de la Bisbal*, 1st ed.; Col·legi d'Aparelladors i Arquitectes tècnics de Girona: Girona, Spain, 2002.
13. Basart, P. 'Nigra sum'. El process de cuita de la terrissa negra explicat per tres quartencs. *Gavarres* **2016**, *30*, 35–82.
14. Associació de Terrissers Artesans de Quart (Ed.) *Paraules que Treballen el fang. Recull de Mots i Locucions dels Oficis de Terrisser i Rajoler a Quart*, 1st ed.; Cossetània Edicions/Museu de la Terrissa de Quart: Quart (Girona), Spain, 2016.
15. Rice, P.M. *Pottery Analysis a Sourcebook*, 1st ed.; The University of Chicago Press: Chicago, IL, USA, 1987.
16. Quinn, P.S.; Benzonelli, A. X-ray diffraction and archaeological materials analysis. In *The SAS Encyclopedia of Archaeological Sciences*, 1st ed.; López Varela, S.L., Ed.; Wiley Blackwell: Hoboken, NJ, USA, 2018.
17. Kùpfér, T.; Maggetti, M. Die Terra Sigillata von La Péniche (Vidy/Lausanne), Schweiz. *Mineral. Petrogr. Mitt.* **1978**, *58*, 189–212.
18. Maggetti, M. Phase analysis and its significance for technology and origin. In *Archaeological Ceramics*, 1st ed.; Olin, J., Franklin, A., Eds.; Smithsonian Institution Press: Washington, DC, USA, 1982; pp. 121–133.
19. Maritan, L. Archaeometric study of Etruscan-Padan type pottery from the Veneto region: Petrographic, mineralogical and geochemical-physical characterization. *Eur. J. Mineral.* **2004**, *16*, 297–307. [[CrossRef](#)]
20. Maritan, L.; Nodari, L.; Mazzoli, C.; Milano, A.; Russo, U. Influence of firing conditions on ceramic products: Experimental study on clay rich in organic matter. *Appl. Clay Sci.* **2006**, *31*, 1–5. [[CrossRef](#)]
21. Maritan, L.; Mazzoli, C.; Freestone, I. Modelling changes in mollusc shell internal microstructure during firing: Implications for temperature estimation in shell-bearing pottery. *Archaeometry* **2007**, *49*, 529–541. [[CrossRef](#)]
22. Viania, A.; Cultrone, G.; Sotiriadis, K.; Ševčíka, R.; Šašeka, P. The use of mineralogical indicators for the assessment of firing temperature in fired-clay bodies. *Appl. Clay Sci.* **2018**, *163*, 108–118. [[CrossRef](#)]
23. Quinn, P.S. *Ceramic Petrography: The Interpretation of Archaeological Pottery and Related Artefacts in Thin Section*, 1st ed.; Archaeopress: Oxford, UK, 2013.
24. Maggetti, M.; Neururer, C.; Ramseyer, D. Temperature evolution inside a pot during experimental surface (bonfire) firing. *Appl. Clay Sci.* **2011**, *53*, 500–508. [[CrossRef](#)]
25. Cau Ontiveros, M.A.; Day, P.M.; Montana, G. Secondary calcite in archaeological ceramics: Evaluation of alteration and contamination processes by thin section study. In *Modern Trends in Scientific Studies on Ancient Ceramics*, 1st ed.; Kilikoglou, V., Hein, A., Maniatis, Y., Eds.; Papers Presented at the 5th European Meeting on Ancient Ceramics, Athens, 1999; BAR International Series 1011; Archaeopress: Oxford, UK, 2002; pp. 9–18.
26. Picon, M. Grises et grises: Quelques réflexions Sur les céramiques cuites en mode B. In *Actas das 1as Jornadas de Cerâmica Medieval e Pós-Medieval. Métodos e Resultados Para o Seu Estudo (1992)*, 1st ed.; Câmara Municipal de Tondela: Porto, Portugal, 1995; pp. 283–292.

27. Price, J.R.; Velbel, M.A. Rates of biotite weathering, and clay mineral transformation and neoformation, determined from watershed geochemical mass-balance methods for the Coweeta Hydrologic Laboratory, Southern Blue Ridge Mountains, North Carolina, USA. *Aquat. Geochem.* **2014**, *20*, 203–224. [[CrossRef](#)]
28. Kularatne, K.U.K.S.; Pitawala, H.M.T.G.A. Leaching of Fluoride from Biotite mica in soil: Implications for fluoride in shallow groundwater. *ISRN Soil Sci.* **2012**, *2012*, 739051. [[CrossRef](#)]
29. Bisdom, E.B.A.; Stoops, G.; Delvigne, J.; Curmi, P.; Altemiller, H.J. Micromorphology of weathering biotite and its secondary products. *Pedologie* **1982**, *32*, 225–252.
30. Eswaran, H.; Heng, Y.Y. The weathering of biotite in a profile on gneiss in Malaysia. *Geoderma* **1976**, *16*, 9–20. [[CrossRef](#)]
31. Wilson, M. A study of weathering in a soil derived from a biotite-hornblende rock. I. Weathering of biotite. *Clay Miner.* **1970**, *8*, 291–303. [[CrossRef](#)]
32. He, Y.T.; Bigham, J.M.; Traina, S.J. Biotite dissolution and Cr(VI) reduction at elevated pH and ionic strength. *Geochim. Et Cosmochim. Acta* **2005**, *69*, 3791–3800. [[CrossRef](#)]
33. Kalinowski, B.E.; Schweda, P. Kinetics of muscovite, phlogopite, and biotite dissolution and alteration at pH-4, room temperature. *Geochim. Cosmochim. Acta* **1996**, *60*, 367–385. [[CrossRef](#)]
34. Gardien, V.; Thompson, A.B.; Grujic, D.; Ulmer, P. Experimental melting of biotite + plagioclase ± muscovite assemblages and implications for crustal melting. *J. Geophys. Res.* **1995**, *100*, 15581–15591. [[CrossRef](#)]
35. Gardien, V.; Thompson, A.B.; Ulmer, P. Melting of Biotite + Plagioclase + Quartz gneisses: The role of H₂O in the stability of amphibole. *J. Petrol.* **2000**, *51*, 651–666. [[CrossRef](#)]
36. Jenkin, G.R.T.; Ellam, R.M.; Rogers, G.; Stuart, F.M. An investigation of closure temperature of the biotite Rb-Sr system: The importance of cation exchange. *Geochim. Cosmochim. Acta* **2001**, *65*, 1141–1160. [[CrossRef](#)]
37. Jiménez-Millán, J.; Vázquez, M.; Velilla, N. Deformation promoted defects and retrograde chloritization of biotite in slates from a shear zone, Southern Iberian Massif, SE Spain. *Clays Clay Miner.* **2007**, *55*, 285–295. [[CrossRef](#)]
38. Walton, E.L.; Sharp, T.G.; Hu, J.; Tschauner, O. Investigating the response of biotite to impact metamorphism: Examples from the Steen River impact structure, Canada. *Meteorit. Planet. Sci.* **2018**, *53*, 75–92. [[CrossRef](#)]
39. Hogg, C.S.; Meads, R.E. A Mössbauer study of thermal decomposition of biotites. *Mineral. Mag.* **1975**, *40*, 79–88. [[CrossRef](#)]
40. Tripathi, R.P.; Chandra, U.; Chandra, R.; Lokanathan, S. A Mössbauer study of the effect of heating biotite, phlogopite and vermiculite. *J. Inorg. Nucl. Chem.* **1978**, *40*, 1293–1298. [[CrossRef](#)]
41. Brearley, A.J. A natural example of the disequilibrium breakdown of biotite at high temperature: TEM observations and comparison with experimental kinetic data. *Mineral. Mag.* **1987**, *51*, 93–106. [[CrossRef](#)]
42. Chon, C.-M.; Kim, S.A.; Moon, H.-S. Crystal structures of biotite at high temperatures and of heat-treated biotite using neutron powder diffraction. *Clays Clay Miner.* **2003**, *51*, 519–528. [[CrossRef](#)]
43. Lagat, J. Hydrothermal Alteration Mineralogy in Geothermal Fields with Case Examples from Olkaria Domes Geothermal Field, Kenya. Presented at Short Course IV on Exploration for Geothermal Resources, Organized by UNU-GTP, KenGen and GDC, Lake Naivasha, Kenya, 1–22 November 2009. Available online: <https://orkustofnun.is/gogn/unu-gtp-sc/UNU-GTP-SC-11-02.pdf> (accessed on 7 December 2020).
44. Papoulis, D.; Tsolis-Katagas, P.; Kalampounias, A.G.; Tsikouras, B. Progressive formation of halloysite from the hydrothermal alteration of biotite and the formation mechanisms of anatase in altered volcanic rocks from Limnos Island, Northeast Aegean Sea, Greece. *Clays Clay Miner.* **2009**, *57*, 566–577. [[CrossRef](#)]
45. Quinn, P.S. (Ed.) *Interpreting Silent Artefacts. Petrographic Approaches to Archaeological Ceramics*, 1st ed.; Archaeopress: Oxford, UK, 2009.
46. Riutort, J.; Cau Ontiverosa, M.A.; Roig i Buxó, J. Archaeometric characterization of regional late antique cooking wares from the area of Vallès (Catalonia, Spain): The case of two rural sites. *J. Archaeol. Sci. Rep.* **2018**, *21*, 1091–1102. [[CrossRef](#)]
47. Riutort, J.; Fantuzzi, L.; Cau Ontiverosa, M.A. Cooking and common wares in the Late Antique rural site of Plaça Major de Castellar del Vallès (Catalonia, Spain): Archaeometric characterization. *Archaeol. Anthropol. Sci.* **2020**, *12*, 106. [[CrossRef](#)]
48. Institut Cartogràfic i Geològic de Catalunya: Mapa Geològic 1:250.000. Available online: <http://icc.cat/vissir3/> (accessed on 4 March 2021).
49. Degen, T.; Sadki, M.; Bron, E.; König, U.; Nénert, G. The HighScore suite. *Powder Diffr.* **2014**, *29*, 13–18. [[CrossRef](#)]
50. Sedmale, G.; Sperberga, I.; Sedmalis, U. Phase composition and properties of mullite ceramic in high temperature testing. In Conference proceedings, symposium Mullite processing, structure, and properties. *Bull. Am. Ceram. Soc.* **1990**, *69*, 1526–1527.
51. Cultrone, G.; Rodríguez-Navarro, C.; Sebastián, E.; Cazalla, O.; De la Torre, M.J. Carbonate and silicate phase reactions during ceramic firing. *Eur. J. Mineral.* **2001**, *13*, 621–634. [[CrossRef](#)]
52. Nodari, L.; Marcuz, E.; Maritan, L.; Mazzoli, C.; Russo, U. Hematite nucleation and growth in the firing of carbonate-rich clay for pottery production. *J. Eur. Ceram. Soc.* **2007**, *27*, 4665–4673. [[CrossRef](#)]
53. Riu, M. Talleres y hornos alfareros de cerámica gris en Cataluña. In *Fours de Potiers et Testares Médiévaux en Méditerranée Occidentale. Méthodes et Résultats*, 1st ed.; Bazzana, A., Amigues, F., Eds.; Colecciones de la casa de Velázquez: Madrid, Spain, 1990; pp. 105–115.
54. Travé, E.; Padilla, J.I. Alfares, hornos y producción de cerámica en la Cataluña medieval y moderna: Una reflexión para su estudio. *Territ. Soc. Y Poder* **2013**, *8*, 105–132.
55. Whitney, D.L.; Evans, B.W. Abbreviations for names of rock-forming minerals. *Am. Mineral.* **2010**, *95*, 185–187. [[CrossRef](#)]

56. Travé, E.; Quinn, P.S.; López, M.D.; Padilla, J.I. One hundred sherds of grey: Compositional and technological characterization of medieval greyware pottery production at Cabrera d’Anoia, Catalonia, Spain. *Archaeol. Anthropol. Sci.* **2014**, *6*, 397–410. [[CrossRef](#)]
57. Thomsen, T.B.; Schmidt, M.W. The biotite to phengite reaction and mica-dominated melting in fluid + carbonate-saturated pelites at high pressures. *J. Petrol.* **2008**, *49*, 1889–1914. [[CrossRef](#)]
58. Pérez-Maqueda, L.A.; Blanes, J.M.; Pascual, J.; Pérez-Rodríguez, J.L. The influence of sonication on the thermal behavior of muscovite and biotite. *J. Eur. Ceram. Soc.* **2004**, *24*, 2793–2801. [[CrossRef](#)]
59. Vedder, W.; Wilkins, R.W.T. Dehydroxylation and rehydroxylation, oxidation and reduction of micas. *Am. Mineral.* **1969**, *54*, 482–509.
60. Maniatis, Y.; Simopoulos, A.; Kostikas, A.; Perdikatsis, V. Effect of Reducing Atmosphere on Minerals and Iron Oxides Developed in Fired Clays: The Role of Ca. *J. Am. Ceram. Soc.* **1983**, *66*, 773–781. [[CrossRef](#)]